Thermoelectric transport in junctions of Majorana and Dirac channels

Dmitriy S. Shapiro,[1,2,3,4,*] D. E. Feldman,[5] Alexander D. Mirlin,[6,7,8] and Alexander Shnirman[7]

[1]*V. A. Kotel'nikov Institute of Radio Engineering and Electronics, Russian Academy of Sciences, Moscow 125009, Russia*
[2]*L. D. Landau Institute for Theoretical Physics, Russian Academy of Sciences, Moscow 117940, Russia*
[3]*Dukhov Research Institute of Automatics (VNIIA), Moscow 127055, Russia*
[4]*Moscow Institute of Physics and Technology, Dolgoprudny 141700, Russia*
[5]*Department of Physics, Brown University, Providence, Rhode Island 02912, USA*
[6]*Institut für Nanotechnologie, Karlsruhe Institute of Technology, 76021 Karlsruhe, Germany*
[7]*Institut für Theorie der Kondensierten Materie, Karlsruhe Institute of Technology, 76128 Karlsruhe, Germany*
[8]*Petersburg Nuclear Physics Institute, St. Petersburg 188300, Russia*

We investigate the thermoelectric current and heat conductance in a chiral Josephson contact on a surface of a three-dimensional topological insulator, covered with superconducting and magnetic insulator films. The contact consists of two junctions of Majorana and Dirac channels next to two superconductors. Geometric asymmetry results in a supercurrent without a phase bias. The interference of Dirac fermions causes oscillations of the electric and heat currents with an unconventional period $2\Phi_0 = h/e$ as functions of the Aharonov-Bohm flux. Due to the gapless character of Majorana modes, there is no threshold for the thermoelectric effect, and the current-flux relationship is nonsinusoidal. Depending on the magnetic flux, the direction of the electric current can be both from the hot to the cold lead and vice versa.

I. INTRODUCTION

A Majorana fermion is simply the real or imaginary part of a complex fermion. At first sight this implies that no meaningful distinction exists between systems of complex and Majorana fermions. However, it is more practical and much more conventional to use the language of complex fermions for normal metals and many other systems. On the other hand, Majorana fermions provide a natural description for various topological materials. The simplest example is the Kitaev chain [1]. Its low-energy degrees of freedom are two Majorana excitations at the chain's ends. Two-dimensional (2D) topological materials bring richer examples of Majorana physics. For example, Majorana edge modes [2] are expected in several candidates states [3,4] for the quantum-Hall effect at the filling factor of 5/2.

If a Majorana system is in contact with a system of complex fermions, then a natural question concerns transformations between the two types of fermions when the systems exchange electrons. The simplest version of that question involves electron tunneling [5–7]. A more interesting setting is a *Y* junction of Majorana modes that merge into a Dirac quantum channel. Such junctions can be built on a surface of a three-dimensional (3D) topological insulator (TI) [8,9].

It has long been known that one-dimensional (1D) charge-neutral Majorana fermions can exist as subgap edge modes of 2D chiral *p*-wave topological superconductors [10,11]. An *s*-wave superconductor (SC) also can give rise to such modes in a partially gapped hybrid structure with a superconducting film on a surface of a TI. A splitted film that hosts an SC-insulator-SC interface on top of a 3D TI supports a gapped nonchiral 1D Majorana mode whereas an SC/ferromagnet junction supports a gapless chiral one (χMM) [8,9]. Recently topological superconductivity and Majorana 1D edge modes were reported in an anomalous quantum-Hall insulator/SC heterostructure [12] and in a single atomic Pb layer on a magnetic Co/Si(111) island [13].

A magnetic domain wall on top of a TI hosts a chiral Dirac mode (χDM). Combinations of such domain walls with SC/magnet junctions allow the implementation of novel quantum devices. The simplest example is a *Y* junction of Majorana and Dirac modes. Other proposals include the Mach-Zehnder [9,14], Fabry-Pérot [15,16], and Hanbury Brown-Twiss [17] quantum interferometers. In our work [18] we introduced a 3D TI-based chiral Josephson contact.

The previous work has focused on electric transport in the above devices. In the present paper we extend this line of research to thermoelectric and thermal transport. Our motivation comes from the question about the nonequilibrium state that forms if two Majorana modes with different temperatures fuse into a Dirac mode. We focus on the setup from Ref. [18] and derive analytical expressions for the thermoelectric and heat currents in the presence of the magnetic field through the normal region. Note that thermal transport between a lead and a 1D Majorana mode has been studied in Ref. [19]. The case of localized Majorana bound states has been studied in Ref. [20].

Our device is shown in Fig. 1. It can be understood as a Fabry-Pérot interferometer made of four chiral *Y* junctions. Each junction converts neutral Majorana fermions into charged Dirac particles. The charge is supplied by a superconductor. The device is a relative of a quantum-Hall-based Josephson junction with a gapped superconductor and a quantum-Hall bar in the normal region [21,22]. In such a structure, the supercurrent is carried by chiral edge states. A recent experimental realization of a quantum-Hall junction involved molybdenum rhenium contacts mediated by a micrometer-sized graphene bar encapsulated in boron nitride [23]. An important feature, common to our setting and the quantum-Hall device, is the spatial separation of electrons
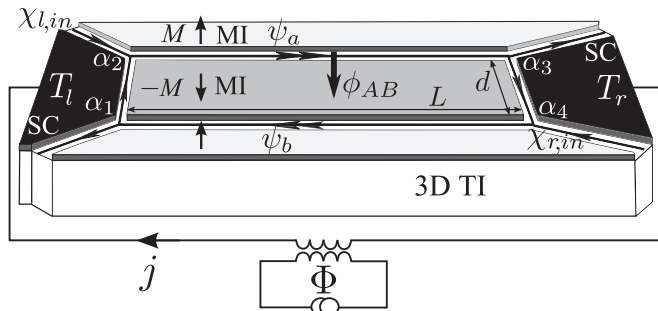
*shapiro.dima@gmail.com

FIG. 1. A chiral Josephson junction on a surface of a 3D topological insulator (3D TI). The lines with a single arrow surrounding black SC films stand for gapless Majorana fermion channels $\chi_{r,l}$, and the arrows show chiralities. Superconducting electrodes have different temperatures T_l and T_r. The light and dark gray areas are magnetic insulators (MIs) which induce exchange fields of the opposite polarizations and energy gaps $\pm M$. Magnetic domain walls support chiral charged modes $\psi_{a,b}$ marked by double arrows. A magnetic flux f in the $-M$ region induces the Aharonov-Bohm phase $\phi_{AB} = \pi f/\Phi_0$.

and holes in Andreev pairs due to the spatial separation of the chiral transport channels. One consequence of such a splitting is a "single-electron" Aharonov-Bohm periodicity in the transport behavior: All transport quantities are periodic in the magnetic flux through the gray region of Fig. 1 with the period $2\Phi_0 = h/e$. For comparison, $S/N/S$ junctions, based on quantum-spin-Hall (or 2D TI) films [24–26] or two-channel nanowires [27], exhibit even-odd transitions between the Φ_0 and the $2\Phi_0$ periodicities. The heat transport and interference effects in thermally biased 2D TI-based Josephson junctions have been studied in Refs. [28,29].

Below we compute the thermal and thermoelectric currents. The time-reversal symmetry is broken by the magnetic film. As a consequence, the inevitable geometric asymmetry of the junction results in a nonzero electric current even in the absence of a temperature gradient, a phase difference between superconductors, and an Aharonov-Bohm flux. The thermoelectric effect requires particle-hole asymmetry. This asymmetry is due to the Aharonov-Bohm effect. Our results reveal a significant difference in thermal transport in the setup of Fig. 1 from the thresholdlike transport in a conventional $S/N/S$ junction with gapped leads. The thermoelectric current oscillates as a function of the Aharonov-Bohm flux and, consequently, as a function of the interferometer area. The oscillation amplitude is geometry dependent. We find the maximal current on the order of $e E_{Th}/\hbar \sim e/\tau$, where E_{Th} is the Thouless energy and τ is the electron travel time through the device if the temperatures of the leads satisfy $T_l \gg E_{Th} \gg T_r$ or $T_r \gg E_{Th} \gg T_l$. The $2\Phi_0$-periodic heat conductance oscillates from zero to one-half of the heat conductance quantum. The maximum heat conductance agrees with what is expected for a fully transparent junction of chiral Majorana channels [30]. Note that the experimental measurement of quantized thermal conductance has recently been accomplished in the integer [31] and fractional [32] quantum-Hall effects.

The width d and length L of the normal region, bounded by two counterpropagating charged χDMs, are much longer than the coherence lengths ξ of the induced superconductivity. Hence, the Thouless energy, proportional to the inverse travel time through the interferometer, is much lower than the superconducting proximity gap and the magnetic exchange gap $E_{Th} \ll \Delta, M$. We assume that the temperatures of the incoming Majorana modes are below those gaps. We will mostly focus on the case of a much higher exchange than superconducting gap $M \gg \Delta$. In this case all contributions to the Josephson current arise from the 1D Dirac channels and do not involve the 2D band between the superconducting leads. Indeed, we expect no contributions to the Josephson effect from the energies $E > M \gg \Delta$. The gray 2D area exhibits insulating behavior for the energies below M, and the tunneling through the insulator is suppressed due to its large size $L \gg \xi$. Another assumption is that the superconducting leads are large and have a constant chemical potential which crosses the Dirac point. This means that the dc Josephson effect in this contact is 2π periodic because the fermion parity is not conserved. The unconventional nonequilibrium 4π-periodic component, predicted in Refs. [1,33–37] for localized zero-energy Majorana bound states [38], is suppressed in our device.

Since we only consider 1D physics, we ignore phonons in the bulk. Phonons are not expected to have much effect on the electric current. They do contribute to the thermal conductance. We are only interested in the oscillating contribution from topological modes. One can isolate it experimentally in a setting where two hot Majorana modes are brought to a cold device.

II. DIRAC AND MAJORANA 1D LIQUIDS

The mean-field Hamiltonian of the 2D structure introduced in Fig. 1 reads

$$
\begin{aligned}
H &= \frac{1}{2} \int dx \, dy \, \Psi^+ h \Psi, \\
h &= i v \tau_z \mathbf{z} \cdot (\boldsymbol{\sigma} \times \boldsymbol{\nabla}) + \tau_0 \sigma_z M(x,y) \\
&\quad + [\tau_+ \Delta(x,y) + \tau_- \Delta^*(x,y)] \sigma_0,
\end{aligned} \tag{1}
$$

where $\boldsymbol{\sigma}$ and $\boldsymbol{\tau}$ are the Pauli matrices in the spin and Nambu spaces. The spinor $\Psi = [\psi_\uparrow, \psi_\downarrow, \psi_\downarrow^+, -\psi_\uparrow^+]^T$ contains field operators of free electrons and holes on the surface of the topological insulator. The helical states of the 2D surface are described by the Rashba Hamiltonian with the Fermi velocity v and the chemical potential $\mu = 0$ crossing the Dirac point. The superconducting s-wave pairing potential is given by $\tau_+ \sigma_0 \Delta(x,y)$, whereas the exchange field of the magnetic insulator films is described by the $\tau_0 \sigma_z M(x,y)$ term. The black areas of right (left) SC contacts have $\Delta(x,y) = \Delta e^{-i\Phi_{r,l}}$. In the normal region filled with magnetic films the magnetization is perpendicular to the 2D surface and changes its sign: In the light gray regions the induced exchange gap $M(x,y) = M$ and in the dark gray rectangle $M(x,y) = -M$. Both M and Δ are real.

An effective 1D Hamiltonian of a Majorana mode, such as the one marked by the single arrow in Fig. 2, was derived by Fu and Kane [9]. This derivation is based on a solution of the 2D Bogolyubov–de Gennes equation. Below we review the
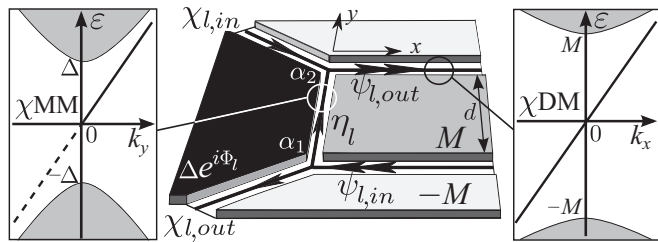
FIG. 2. The structure of the chiral Dirac-Majorana 1D contact formed by two Y junctions. The film of a superconductor with the phase of the order parameter Φ_l and magnetic insulators of the opposite magnetizations induce proximity Δ and exchange gaps $\pm M$ on the 2D helical surface. The boundaries between the superconductors and the magnets support the chiral charged modes $\psi_{\text{in,out}}$ and the neutral modes $\chi_{\text{in,out}}$ and η_l.

solution for the mode η which connects Y junctions 1 and 2 in Fig. 2 and propagates along the SC/magnet interface at $x = 0$. In the SC region (the $x < 0$ half plane), there is an s-wave SC pairing potential given by $\Delta(x,y) = \Delta e^{i\Phi_l}\theta(-x)$, whereas at $x > 0$ the magnetic film induces the exchange gap $M(x,y) = -M\,\theta(x)$. There exists a 1D solution of the Bogolyubov–de Gennes equation $h\xi_{k_y} = \varepsilon_{k_y}\xi_{k_y}$ such that the wave function decays exponentially in the directions, normal to the SC/magnet interface as $\sim \exp[-|(\theta(x)M - \theta(-x)\Delta)x|/(\hbar v)]$ and is a plane wave with the momentum k_y along the boundary. This 1D chiral mode with the dispersion relation,

$$\varepsilon_{k_y} = -\text{sgn}(M)vk_y \qquad (2)$$

is *nondegenerate* within the gap, i.e., for $\varepsilon_{k_y} < \min(\Delta, M)$, but continues to exist also for higher energies. The eigenvectors are self-conjugate $\xi_{k_y} = \sigma_y\tau_y\xi^*_{-k_y}$, which is consistent with the fact that the field Ψ is self-charge-conjugate $\Psi = \sigma_y\tau_y\Psi^*$. Hence, the Bogolyubov quasiparticle operator,

$$\eta_{k_y} = \int dx\, dy[\xi_{k_y}(x,y)]^\dagger \Psi(x,y) \qquad (3)$$

is real, $\eta_{k_y} = \eta^+_{-k_y}$, and describes a chiral Majorana mode.

The normal region with Dirac modes is confined by domain walls where the magnetization sign changes (the horizontal lines marked by the double arrows in Fig. 2). To derive the effective 1D Hamiltonian for those modes from the 2D Hamiltonian in the Nambu space (1), we set $\Delta(x,y) = 0$ and focus on the mass term $M(x,y) = M\,\text{sgn}(y)$ at $y \approx 0$.

The eigenvalues ε_{k_x} of the Bogolyubov–de Gennes Hamiltonian are now *doubly* degenerate in contrast to the case of χMM. We denote two orthogonal degenerate eigenstates as ζ_{e,k_x} and ζ_{h,k_x} and associate them with electrons and holes. Their wave functions are related via the charge-conjugation constraint as $\zeta_{h,k_x} = \sigma_y\tau_y\zeta^*_{e,-k_x}$. The dispersion relation is the same as for the Majorana channels: $\varepsilon_{k_x} = -\text{sgn}(M)vk_x$. The difference from the neutral mode consists of the existence of two independent excitations of the same energy ε_{k_x} in the Nambu space: an electron of momentum k_x and a hole of momentum $-k_x$. In terms of Bogolyubov operators this is the Dirac gapless mode described by a complex field. In the second quantization language, the electron and hole operators

are given by

$$\psi_{e,k_x} = \int dx\, dy[\zeta_{e,k_x}(x,y)]^\dagger \Psi(x,y), \qquad (4)$$

and

$$\psi_{h,k_x} = \int dx\, dy[\zeta_{h,k_x}(x,y)]^\dagger \Psi(x,y). \qquad (5)$$

They are not independent since $\psi_{h,k_x} = \psi^+_{e,-k_x}$ due to the charge-conjugation constraints for $\Psi(x,y)$ and $\zeta_{e,k_x}, \zeta_{h,k_x}$. In what follows we do not use $\psi_{h,e}$ and instead introduce the field ψ_{k_x} such that $\psi_{e,k_x} = \psi_{k_x}$ and $\psi_{h,k_x} = \psi^+_{-k_x}$.

At this point we are in the position to write down effective 1D Hamiltonians for free Majorana and Dirac particles. The secondary quantized Ψ operators of these 1D modes are as follows:

$$\Psi_M(x,y) = \int \frac{dk_y}{2\pi}\xi_{k_y}(x,y)\eta_{k_y} \qquad (6)$$

for χMM and

$$\Psi_D(x,y) = \int \frac{dk_x}{2\pi}[\zeta_{e,k_x}(x,y)\psi_{k_x} + \zeta_{h,k_x}(x,y)\psi^+_{-k_x}] \qquad (7)$$

for χDM. Integrating out the y coordinate in the Bogolyubov–de Gennes Hamiltonian yields the effective Hamiltonians of the Majorana modes,

$$H_M = \text{sgn}(M)\frac{iv}{2}\int \eta(y)\partial_y\eta(y)dy, \qquad (8)$$

and the Dirac modes,

$$H_D = \text{sgn}(M)iv\int \psi^+(x)\partial_x\psi(x)dx, \qquad (9)$$

where we introduced the 1D operators,

$$\eta(y) = \eta^+(y) = \int \frac{dk_y}{2\pi}\eta_{k_y}e^{ik_y y}, \qquad (10)$$

and

$$\psi(x) = \int \frac{dk_x}{2\pi}\psi_{k_x}e^{ik_x x}, \qquad (11)$$

which describe coherent propagation of neutral and charged fermions through 1D guiding channels with the Fermi velocity v. For $M > 0$ the chiralities of the 1D modes are shown by the arrows in Figs. 1 and 2. The factor of $1/2$ in the Majorana Hamiltonian H_M reflects the fact that the negative and positive energy excitations in the χMM are not independent. In other words, the lower branch of the dispersion $\varepsilon_{k_y} = -\text{sgn}(M)vk_y$ at $k_y < 0$ is redundant (it is shown as a dashed line in the left inset of Fig. 2). The coefficient $1/2$ implies that a neutral Majorana fermion carries only a half of the heat current of a Dirac mode at the same temperature so that the ballistic heat conductance G_0 of a single χMM is one-half of the heat conductance quantum,

$$G_0 = \frac{1}{2}\frac{\pi^2 k_B^2 T}{3h}, \qquad (12)$$

where T is the temperature.

III. SCATTERING IN A MAJORANA-DIRAC CONTACT

The normal region includes a rectangular magnetic film (dark gray area in Fig. 1) of the length L and the width d. L and d exceed significantly both the SC and the magnetic coherence lengths $d, L \gg \hbar v/\Delta, \hbar v/M$. Four Y junctions are in the corners of the film. A single Y junction is formed by two Majorana and one Dirac channels (Fig. 2). The angles between the channels as well as other microscopic details are not necessarily the same in different Y junctions.

We start with the calculation of the scattering matrix describing two nonidentical Y junctions shown in Fig. 2 (see Ref. [18]). This scattering matrix describes the coupling between χMMs on the SC/magnet interfaces and two 1D Dirac modes. Specifically, it provides a relation between the operators of incoming and outgoing electrons and holes $\psi_{\text{in,out}}, \psi_{\text{in,out}}^+$ of χDM (horizontal lines marked by double arrows) and $\chi_{\text{in,out}}$ of semi-infinite neutral χMMs (lines marked by single arrows). The 1D modes, described by the wave-functions ξ and $\zeta_{e,h}$, are spin nondegenerate and have in-plane spin textures. Hence, the conversion between Majorana and Dirac modes in Y junctions is accompanied by spin rotation. Thus, scattering in a Y junction involves a geometric Berry phase, which is encoded in the phase α below. The calculation of α for a given geometry is straightforward.

Scattering in the upper and lower Y junctions in Fig. 2 is described by the S_{out} and S_{in} matrices, which were found in Refs. [9,14],

$$
\begin{bmatrix} \eta_{l,\text{out}} \\ \chi_{l,\text{out}} \end{bmatrix} = S_{in,\alpha_1} \begin{bmatrix} \psi_{l,\text{in}} \\ \psi_{l,\text{in}}^+ \end{bmatrix}, \qquad \begin{bmatrix} \psi_{l,\text{out}} \\ \psi_{l,\text{out}}^+ \end{bmatrix} = S_{out,\alpha_2} \begin{bmatrix} \eta_{l,\text{in}} \\ \chi_{l,\text{in}} \end{bmatrix}.
\tag{13}
$$

Note that the operators in (13) correspond to the incoming and outgoing scattering states rather than to free plane waves of (3)–(5) [39].

Let us assume first that $\Phi_l = 0$ in the electrode. A nonzero Φ_l will be included in a final expression for the S matrix by means of a gauge transformation of Dirac ψ operators. The matrix S_{in,α_1} involves the phase difference α_1 between an electron and a hole converting into two Majorana fermions. The matrix S_{out,α_2} involves a phase α_2 accumulated under merging two Majoranas into a Dirac fermion. The structure of S_{out} is related to that of S_{in} by a time-reversal transformation [14]: $S_{\text{out}} = S_{\text{in}}^T$. The expression for the S_{in} matrix of the lower Y junction is

$$
S_{in,\alpha_1} = \begin{bmatrix} 1/\sqrt{2} & 1/\sqrt{2} \\ i/\sqrt{2} & -i/\sqrt{2} \end{bmatrix} \begin{bmatrix} e^{i\alpha_1} & 0 \\ 0 & e^{-i\alpha_1} \end{bmatrix}.
\tag{14}
$$

Note that, although the phase α_1 can be gauged easily out if the Y junction is considered on its own, it becomes important once several Y junctions are combined into a circuit.

In Ref. [18] the symmetry of four Y junctions ($\alpha_i = \alpha$) was assumed. In this paper we consider an arbitrary set of the phases α_i. We will see that this modifies the current-phase relation in such a way that a nonzero current may flow at a zero external phase bias Φ, such as in Josephson φ-junction devices [40–44].

We proceed by matching the Majorana operators $\eta_{l,\text{in}}$ and $\eta_{l,\text{out}}$ at a given energy ε as $\eta_{l,\text{in},\varepsilon} = e^{ik_\varepsilon} \eta_{l,\text{out},\varepsilon}$. The dynamic phase $k_\varepsilon = \varepsilon d/v$ is accumulated by a Majorana excitation during the propagation from the lower to upper Y junctions, separated by the distance d. The full S_{α_1,α_2} matrix of the contact, acting on $(\psi_{in,\varepsilon}, \chi_{in,\varepsilon}, \psi_{in,-\varepsilon}^+)^T$, can be found after the exclusion of η from Eqs. (13) and is defined by the equation,

$$
\begin{bmatrix} \psi_{l,\text{out},\varepsilon} \\ \chi_{l,\text{out},\varepsilon} \\ \psi_{l,\text{out},-\varepsilon}^+ \end{bmatrix}
$$

$$
= \begin{bmatrix} \frac{1}{2} e^{ik_\varepsilon + i(\alpha_1+\alpha_2)} & \frac{ie^{i\alpha_2}}{\sqrt{2}} & \frac{1}{2} e^{ik_\varepsilon - i(\alpha_1-\alpha_2)} \\[8pt] \frac{ie^{i\alpha_1}}{\sqrt{2}} & 0 & -\frac{ie^{-i\alpha_1}}{\sqrt{2}} \\[8pt] \frac{1}{2} e^{ik_\varepsilon + i(\alpha_1-\alpha_2)} & -\frac{ie^{-i\alpha_2}}{\sqrt{2}} & \frac{1}{2} e^{-i(\alpha_1+\alpha_2)} \end{bmatrix}
$$

$$
\times \begin{bmatrix} \psi_{l,in,\varepsilon} \\ \chi_{l,in,\varepsilon} \\ \psi_{l,in,-\varepsilon}^+ \end{bmatrix}.
\tag{15}
$$

To account for a nonzero SC phase Φ_{SC} of an electrode (colored black in Fig. 2), we employ the transformation $\psi \to e^{i\Phi_{SC}/2}\psi$. For the left contact in Fig. 1 this yields

$$
S_l = C(-\Phi_l)S(\alpha_1,\alpha_2)C(\Phi_l),
\tag{16}
$$

whereas for the scattering matrix for the right contact it gives

$$
S_r = C^{-1}(\Phi_r)S(\alpha_3,\alpha_4)C(\Phi_r).
\tag{17}
$$

Here we have introduced an auxiliary matrix,

$$
C(\Phi_{SC}) = \begin{bmatrix} e^{i\Phi_{SC}} & 0 & 0 \\ 0 & 1 & 0 \\ 0 & 0 & e^{-i\Phi_{SC}} \end{bmatrix}.
\tag{18}
$$

The above $S_{l,r}$ matrices describe partial Andreev reflection in spinless 1D Dirac channels and the creation of excitations in neutral Majorana modes. The Andreev part of this process is accompanied by a Cooper pair absorption in a SC electrode.

We transform the $S_{l,r}$ matrices acting on $\psi_{l,\text{in}}, \psi_{l,\text{out}}$ ($\psi_{r,\text{in}}, \psi_{r,\text{out}}$) on the left (right) ends of the Dirac channels into new matrices $\tilde{S}_{l,r}$, acting on the operators ψ_a, ψ_b in the geometric centers of the 1D channels. The S and $\tilde{S}$ operators are related by a phase shift by the sum of the dynamical phase $\frac{\varepsilon L}{2\hbar v}$, accumulated by an electron of energy ε over the distance $L/2$, and an Aharonov-Bohm phase. For the upper a arm the relation of the scattering matrices can be deduced from the equation,

$$
\psi_{a,\varepsilon} = \exp\left(i\frac{\varepsilon L}{2\hbar v} + i\phi_{AB}/4 \right) \psi_{l,\text{out},\varepsilon}.
\tag{19}
$$

We assume here that the same Aharonov-Bohm phases are accumulated on each portion of the Dirac channels of the same length. The scattering matrices, acting on the ψ operators in

the centers of the channels, take the form

$$\tilde{S}_{l,r} = C\left(\frac{\phi_{AB}}{4}\right)D\left(\frac{\varepsilon L}{2v}\right)S_{l,r}D\left(\frac{\varepsilon L}{2v}\right)C\left(\frac{\phi_{AB}}{4}\right), \quad (20)$$

where ϕ_{AB} is the total Aharonov-Bohm phase. The dynamical phases are encoded in (20) via the matrix,

$$D\left(\frac{\varepsilon L}{2\hbar v}\right) = \begin{bmatrix} \exp\left(i\frac{\varepsilon L}{2\hbar v}\right) & 0 & 0 \\ 0 & 1 & 0 \\ 0 & 0 & \exp\left(i\frac{\varepsilon L}{2\hbar v}\right) \end{bmatrix}. \quad (21)$$

The difference in the above expression from the C matrix is that the first and third diagonal components coincide: The dynamical phases are equal for an electron of the energy ε and a hole of the energy $-\varepsilon$. We can exclude α_i from the diagonal terms of the S matrices by redefining the superconducting phase bias Φ and the Aharonov-Bohm phase ϕ_{AB}. To do that we introduce the phases,

$$\phi_l = \frac{\alpha_1 + \alpha_2}{2}, \quad \phi_r = \frac{\alpha_3 + \alpha_4}{2}, \quad (22)$$

and

$$\varphi_0 = \frac{\Phi_l + \Phi_r}{2}. \quad (23)$$

We can always shift both superconducting phases by the same constant. It will be convenient to shift them so that

$$\varphi_0 = \frac{\alpha_2 - \alpha_1 + \alpha_4 - \alpha_3}{4}. \quad (24)$$

With this choice we find

$$S_l = C[\phi_l - (\Phi + \varphi)/2]S_0 C[\phi_l + (\Phi + \varphi)/2], \quad (25)$$

and

$$S_r = C[\phi_r + (\Phi + \varphi)/2]S_0 C[\phi_r - (\Phi + \varphi)/2], \quad (26)$$

where $S_0 \equiv S_{\alpha_1 = \alpha_2 = 0}$ (15),

$$\Phi = \Phi_l - \Phi_r$$

is the SC phase bias, and the phase shift,

$$\varphi = \tfrac{1}{2}(\alpha_1 - \alpha_2 - \alpha_3 + \alpha_4). \quad (27)$$

It follows from this representation of $S_{l,r}$ and $\tilde{S}_{l,r}$ that the superconducting phase cannot be gauged out by the Aharonov-Bohm phase. We also observe that $\phi_{l,r}$ and ϕ_{AB} enter the C matrices in the same way, and hence, $\phi_{l,r}$ can be gauged out by redefining the total Aharonov-Bohm phase as

$$\phi_{AB} \to \phi_{AB} + 2(\phi_l + \phi_r) = \sum_{i=1}^{4} \alpha_i + \phi_{AB}. \quad (28)$$

IV. JOSEPHSON CURRENT

In our formalism the operators of Dirac fermions are expressed as linear combinations of uncorrelated field operators $\chi_l \equiv \chi_{l,\text{in}}$ and $\chi_r \equiv \chi_{r,\text{in}}$ of incident Majorana modes. The latter are characterized by the Fermi distribution functions,

$$n_{l,r}(\varepsilon) = \frac{1}{2}\left(1 - \tanh\frac{\varepsilon}{2T_{l,r}}\right), \quad (29)$$

i.e.,

$$\langle \chi_{\varepsilon,i}^{\dagger}\chi_{\varepsilon,j}\rangle = v^{-1}\delta_{i,j}n_i(\varepsilon), \quad (30)$$

where the Fourier-transformed operators,

$$\chi_{\varepsilon,i} = \chi_{-\varepsilon,i}^{\dagger} = \int \chi_i(t)e^{i\varepsilon t}dt, \quad (31)$$

and the index $i = l,r$ stands for the left and right incident modes and v^{-1} is the density of states in the χMM channels. We assume $k_B = 1$ everywhere and recover it in the final expressions. The linear spectrum of 1D Dirac modes means that the chiral current is proportional to the charge-density $j_{a,b} = -ev\rho_{a,b}$ and, hence, the current j is given by the integral over energies,

$$j = \int \frac{d\varepsilon}{2\pi\hbar}(-ev)(\langle \psi_{a,\varepsilon}^{+}\psi_{a,\varepsilon}\rangle - \langle \psi_{b,\varepsilon}^{+}\psi_{b,\varepsilon}\rangle). \quad (32)$$

Here $\psi_{a,\varepsilon}$ and $\psi_{b,\varepsilon}$ are the electron operators in the centers of the Dirac channels, and the positive direction of the current is defined from the left to the right.

The S matrices are used to express the Dirac fermion operators in Eq. (32) in terms of the incoming Majorana modes,

$$\psi_{a,\varepsilon} = \frac{i\sqrt{2}\exp\left[\frac{1}{4}i\left(\frac{2L\varepsilon}{v} + \phi - \Phi - \varphi\right)\right]}{1 + 2e^{i\phi}\cos(\Phi + \varphi) + e^{2i\phi} - 4e^{i(\phi - \varphi_\varepsilon)}}$$
$$\times \Big[(1 + e^{i(\Phi + \varphi + \phi)} - 2e^{i(\phi - \varphi_\varepsilon)})\chi_l$$
$$- 2ie^{i\phi - i(1/2)\varphi_\varepsilon}\sin\left(\frac{\Phi + \varphi + \phi}{2}\right)\chi_r\Big], \quad (33)$$

with

$$\phi = \phi_{AB} + \sum_{i=1}^{4}\alpha_i. \quad (34)$$

Due to the symmetry between the a and the b arms we get a similar expression for ψ_b with $\Phi \to -\Phi$, $\varphi \to -\varphi$ and the interchanged χ_l and χ_r. This expression for Dirac operators is a straightforward generalization of that from Ref. [18] to our asymmetric setup: (i) The sum of the phases α_i shifts the total Aharonov-Bohm phase (34), and (ii) the phase φ, introduced in (27), shifts the external superconducting phase bias Φ.

With the use of the expressions for Dirac operators in the N region (33) we obtain that the current can be represented as

$$j = j_t + j_\Phi, \quad (35)$$

where j_t is induced by the temperature gradient and j_Φ generalizes the Josephson current from Ref. [18] to a two-temperature situation. The two contributions read as

$$j_t = \int \frac{d\varepsilon}{2\pi\hbar}(-e)\frac{n_l(\varepsilon) - n_r(\varepsilon)}{2}J_{t,\varepsilon}, \quad (36)$$

and

$$j_\Phi = \int \frac{d\varepsilon}{2\pi\hbar}(-e)\frac{n_l(\varepsilon) + n_r(\varepsilon)}{2}J_\varepsilon. \quad (37)$$

The thermoelectric part (36) is given by a rapidly convergent integral due to the factor of $(n_l - n_r)$. If $T_l = T_r$, then $j_t = 0$, and the total current (35) is given by the Josephson term j_Φ. We calculate j_Φ in this section and analyze j_t in the next one.

The spectral current J_ε, entering into j_Φ, reads

$$J_\varepsilon = \frac{\sin \varphi_\varepsilon \sin(\Phi + \varphi)}{1 + \left(\frac{\cos \phi + \cos(\Phi + \varphi)}{2}\right)^2 - [\cos(\Phi + \varphi) + \cos \phi] \cos \varphi_\varepsilon},$$

(38)

with $\varphi_\varepsilon = \varepsilon/E_{Th}$ being the dynamical phase, accumulated by an excitation of the energy ε on the closed path that connects all four Y junctions. Note that the Josephson term (37) does not converge at high ε and a regularization is needed. Indeed, the spectral current (38) depends periodically on the energy due to the 1D nature of the chiral modes carrying the current. On physical grounds we expect this dependency to be replaced by a slowly decaying (and oscillating) one once the energy ε reaches the lowest border of the 2D continuum $\min(\Delta, M) \gg E_{Th}$. We, thus, smoothly cut off the integration in (37) at $\varepsilon \gg E_{Th}$ which leads to the following current-phase relationship for equal $T_l = T_r = T$:

$$j_\Phi = 4\pi \frac{e k_B T}{h} \sin(\Phi + \varphi)$$
$$\times \sum_{n=0}^{\infty} \frac{1}{2 \exp\left(\pi \frac{k_B T(1+2n)}{E_{Th}}\right) - \cos \phi - \cos(\Phi + \varphi)}.$$

(39)

The phase ϕ shifts the (h/e)-periodic pattern of critical current-flux oscillations, whereas φ results into a nonzero Josephson current without phase bias. The result for different temperatures $T_l \neq T_r$ equals half the sum of the two expressions (39) taken at $T = T_l$ and at $T = T_r$, respectively.

To further support the validity of this regularization procedure based on smooth cutoff, we can perform the derivation in a slightly different way that leads to the same result. Specifically, this alternative—but equivalent—regularization procedure amounts to subtracting and adding a high-temperature Josephson current at $T_l = T_r \gg E_{Th}$. The difference in the Josephson current and the counterterm converges. At the same time, the counterterm is expected to be negligible on physical grounds. Indeed, the Josephson effect is possible due to the particle-hole coherence between the two Dirac channels. Such coherence extends to the length scales on the order of the thermal length $hv/(k_B T)$. For $T \gg E_{Th}$ the thermal length is much shorter than the distance L between the superconductors. Thus, the high-temperature Josephson effect is suppressed. This agrees with the results for $S/N/S$ structures where the normal region is a long quantum wire [45–49]. We emphasize once again that the convergence subtlety discussed here relates to the Josephson current only. The thermoelectric and the heat currents discussed below are given by convergent integrals.

V. THERMOELECTRIC CURRENT

Below we focus on the thermoelectric effect. Thus, we take $T_l \neq T_r$ and set the SC phase bias $\Phi = -\varphi$ so that the Josephson current is $j_\Phi = 0$ in (35). Recall that we have redefined the Aharonov-Bohm phase ϕ in Eq. (34). We investigate the current j_t as a function of two temperatures $T_{l,r}$ and of ϕ. We use the scattering matrices to express the $\psi_{a,\varepsilon}$ operator at $\Phi = -\varphi$ in the center of the upper Dirac channel
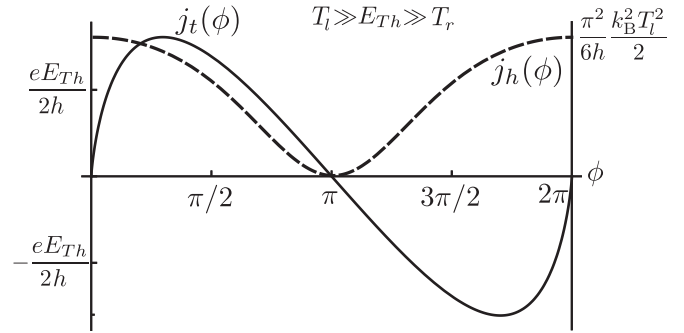

FIG. 3. The thermoelectric current $j_t(\phi)$ and the heat current $j_h(\phi)$ as functions of the flux ϕ at $T_l \gg E_{Th} \gg T_r$.

as we use the expression (33) for the $\psi_{a,\varepsilon}$ operator at $\Phi = -\varphi$ in the center of the upper Dirac channel,

$$\psi_{a,\varepsilon} = i\sqrt{2} e^{(1/4)i[(2L\varepsilon/v) + \phi]}$$
$$\times \frac{(e^{i\varphi_\varepsilon} + e^{i(\varphi_\varepsilon + \phi)} - 2e^{i\phi})\chi_l - (e^{i\phi} - 1)e^{(1/2)i(\varphi_\varepsilon + \phi)}\chi_r}{e^{i\varphi_\varepsilon}(1 + e^{i\phi})^2 - 4e^{i\phi}}.$$

(40)

The ψ_b is given by the interchanged χ_l and χ_r for the rectangular geometry of the N region.

The above operator relations (40) allow the calculation of the dimensionless spectral current $J_{t,\varepsilon}$ entering j_t Eq. (36),

$$J_{t,\varepsilon} = \frac{(1 + \cos \phi)(1 - \cos \varphi_\varepsilon) - \sin \phi \sin \varphi_\varepsilon}{1 + \left(\frac{1 + \cos \phi}{2}\right)^2 - (1 + \cos \phi) \cos \varphi_\varepsilon}.$$

(41)

The term $(1 + \cos \phi)(1 - \cos \varphi_\varepsilon)$ in (41) is an even function of ε and does not contribute to the integral (36) which is evaluated by means of the summation over the residues of $\tanh[\varepsilon/(2T_{l,r})]$. Finally, for arbitrary temperatures and ϕ we obtain an expression for the thermoelectric current,

$$j_t = \frac{k_B e}{\hbar} \sin \phi \sum_{n=0}^{\infty} \left(\frac{T_r}{2 \exp\left(\frac{\pi k_B T_r(1+2n)}{E_{Th}}\right) - 1 - \cos \phi}\right.$$
$$\left. - \frac{T_l}{2 \exp\left(\frac{\pi k_B T_l(1+2n)}{E_{Th}}\right) - 1 - \cos \phi}\right).$$

(42)

We focus on the regime of $T_l \gg E_{Th} \gg T_r$ or $T_r \gg E_{Th} \gg T_l$. We expect the maximal current to be achieved in that region (see the solid curve in Fig. 3). In those cases the terms in the sum (42) with the higher of the two temperatures are exponentially small. The sum of the remaining terms reduces to the integral $T \sum \to E_{Th} \int dx$, where $x = T/E_{Th}$ and T is the smaller of T_r and T_l. The integral is proportional to $e E_{Th}/\hbar$,

$$j_{t,max} = \text{sgn}(T_l - T_r) \frac{e E_{Th}}{2\pi \hbar} \tan \frac{\phi}{2} \ln \frac{2}{1 - \cos \phi}.$$

(43)

Note the divergent derivative $\partial_\phi j_{max}(\phi)$ at $\phi = 2\pi n$.

In the high-temperature regime, where $T_l, T_r \gg E_{Th}$, the thermoelectric current is exponentially suppressed and exhibits a sinusoidal dependence on ϕ,

$$j = \frac{k_B e}{2\hbar} \sin \phi (T_r e^{-\pi T_r/E_{Th}} - T_l e^{-\pi T_l/E_{Th}}).$$

(44)

Similar to the electric current, the thermoelectric current decays exponentially at $k_B T_{l,r} \gg E_{Th}$. This is the limit where the thermal length becomes much less than the interferometer size.

We next briefly address a general situation with nonzero Josephson and thermoelectric currents. We derive from (33) that $J_{t,\varepsilon}$, entering the thermoelectric contribution (36), reads for arbitrary temperatures, superconducting phases, and Aharonov-Bohm phases as

$$J_{t,\varepsilon}(\Phi)$$
$$= \frac{1 + (\cos\phi - \cos\varphi_\varepsilon)\cos(\Phi + \varphi) - \cos(\phi - \varphi_\varepsilon)}{1 + \left(\frac{\cos\phi + \cos(\Phi+\varphi)}{2}\right)^2 - [\cos(\Phi + \varphi) + \cos\phi]\cos\varphi_\varepsilon}.$$
(45)

Comparing the above equation (45) with J_ε from (37) we relate the thermoelectric current j_t and the Josephson currents $j_\Phi(T_{r,l})$ (39),

$$j_t = \frac{\sin\phi}{2\sin(\Phi + \varphi)}[j_\Phi(T_r) - j_\Phi(T_l)].$$
(46)

At $T_r \neq T_l$, the Josephson current reads

$$j_\Phi = \tfrac{1}{2}[j_\Phi(T_r) + j_\Phi(T_l)].$$
(47)

Figure 4 shows the bias dependencies of the thermoelectric and Josephson currents at the Aharonov-Bohm phase $\phi = \pi/3$ in three temperature domains: (a) $T_{r,l} < E_{Th}$, (b) $T_l > E_{Th} > T_r$, and (c) $T_{r,l} > E_{Th}$. In regime (a) the Josephson part is maximal, but the thermoelectric effect is suppressed. In (b) and (c) the thermal and Josephson parts are of the same orders of magnitude $j_t \sim j_\Phi$. From (c) we see that the dependence of j_t on Φ vanishes at high temperatures.

Below we compute the bias phase Φ^* which results in zero total current,

$$j(\Phi^*, T_r, T_l) = 0.$$
(48)

This value of the phase can be seen as an analog of thermovoltage in the Josephson effect. In this regime (48) where the Josephson and thermal currents compensate each other, one finds

$$j_{\Phi^*} = -j_t.$$
(49)

From (46), (47), and (49) we obtain an equation on Φ^*,

$$\sin(\Phi^* + \varphi) = \frac{j_{\Phi^*}(T_l) - j_{\Phi^*}(T_r)}{j_{\Phi^*}(T_l) + j_{\Phi^*}(T_r)}\sin\phi,$$
(50)

where j_Φ was introduced in (39).

The relation between Φ^* and the temperature gradient $\Delta T = T_r - T_l$ is nonlinear. Let us consider several limiting cases of (50) and their solutions. The first one is the high-temperature limit with $T_r, T_l \gg E_{Th}$. In this case the currents are

$$j_\Phi(T_{l,r}) = 2\pi \frac{e k_B T_{l,r}}{h} \exp\left(-\frac{\pi T_{l,r}}{E_{Th}}\right)\sin(\Phi + \varphi),$$
(51)

and the solution for Φ^* reads

$$\Phi^* = \arcsin\left(\sin\phi \tanh\frac{\pi(T_r - T_l)}{2E_{Th}}\right) - \varphi.$$
(52)

(a) $\frac{eE_{Th}}{h}$ $T_l = 0.2E_{Th}$ $T_r = 0.1E_{Th}$ $\phi = \pi/3$

(b) $\frac{eE_{Th}}{h}$ $T_l = 2E_{Th}$ $T_r = 0.1E_{Th}$

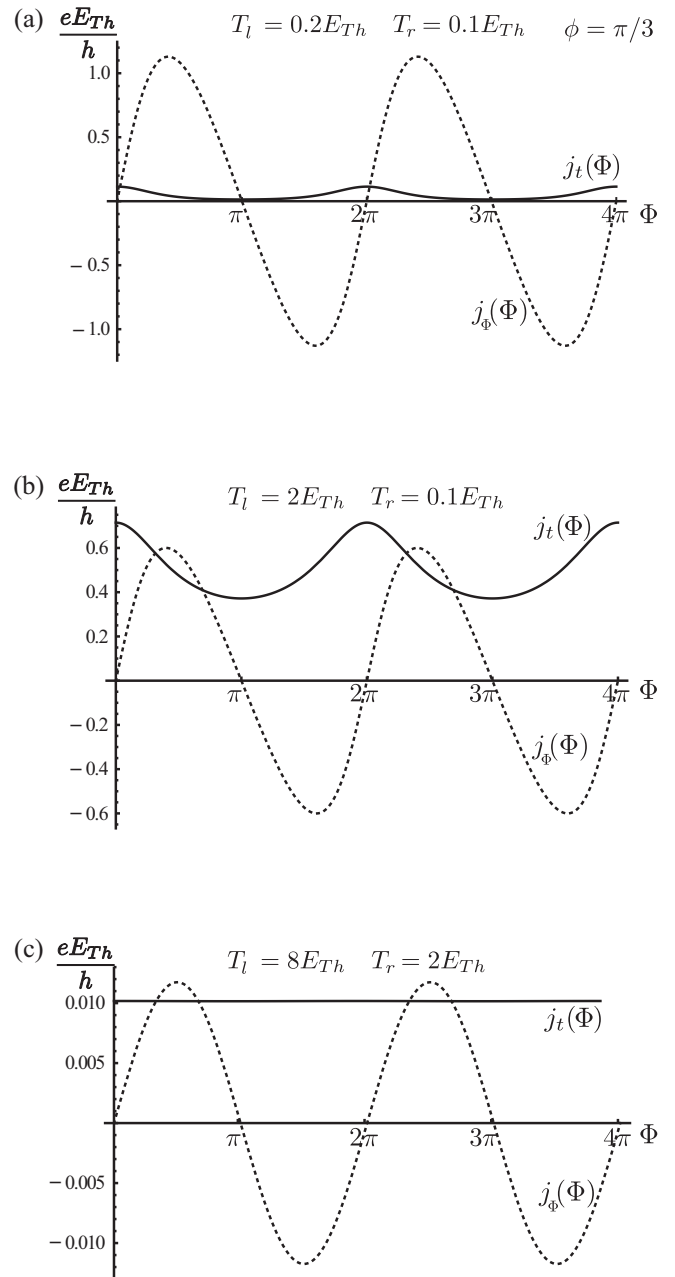(c) $\frac{eE_{Th}}{h}$ $T_l = 8E_{Th}$ $T_r = 2E_{Th}$

FIG. 4. The thermoelectric $j_t(\Phi)$ and Josephson $j_\Phi(\Phi)$ parts of the current as functions of the superconducting phase Φ with the phase φ set to zero. The Aharonov-Bohm phase is $\phi = \pi/3$.

In the limits of $T_l \gg E_{Th} \gg T_r$ or $T_r \gg E_{Th} \gg T_l$, one of the currents in (50) is temperature independent and is given by $j_\Phi \propto E_{Th}$, whereas the other is exponentially suppressed as in (51). The result is

$$\Phi^* = \phi \, \mathrm{sgn}(T_r - T_l) - \varphi.$$
(53)

In the low-temperature limit $T_r, T_l \ll E_{Th}$, for small gradients $\Delta T \ll T \ll E_{Th}$, we obtain that

$$\Phi^* = \frac{\Delta T}{3} \frac{\pi^2 k_B^2 T}{E_{Th}^2} \frac{(1 + \cos\phi)\sin\phi}{(1 - \cos\phi)^2 \ln\frac{2}{1-\cos\phi}} - \varphi,$$
(54)

with $\Delta T = T_r - T_l$.

VI. HEAT CURRENT

The energy current at $\Phi = -\varphi$ is defined analogous to the thermoelectric one (36) with the replacement of the electron charge by the energy $(-e) \rightarrow \varepsilon$,

$$j_h = \int \frac{d\varepsilon}{2\pi\hbar} \varepsilon \frac{n_l(\varepsilon) - n_r(\varepsilon)}{2} J_{t,\varepsilon}. \tag{55}$$

The part in $J_{t,\varepsilon}$ (41), which is proportional to $\sin\phi \sin\varphi_\varepsilon$ and contributes to j_t, does not contribute to j_h, whereas the term $\sim (1 + \cos\phi)(1 - \cos\varphi_\varepsilon)$ from $J_{t,\varepsilon}$ does contribute to the energy current. The result of the integration at an arbitrary temperatures reads

$$j_h = \frac{\pi^2 k_{\mathrm{B}}^2}{6h} \frac{1 + \cos\phi}{3 + \cos\phi} (T_l^2 - T_r^2) + \pi^2 \frac{1 - \cos^2\phi}{3 + \cos\phi}$$
$$\times \sum_{n=0}^{\infty} \left(\frac{k_{\mathrm{B}}^2 T_r^2 (2n+1)/h}{\exp\left[\frac{\pi k_{\mathrm{B}} T_r(1+2n)}{E_{Th}}\right] - \cos^2(\phi/2)} - (T_r \rightarrow T_l) \right). \tag{56}$$

The first term in (56) gives a ballistic contribution to the heat conductance modulated by ϕ. The heat current is h/e periodic like the electric current, but the energy current has always the same sign in contrast to the electric current j_t. In the limit of $T_l \gg E_{Th} \gg T_r$ the amplitude of the heat current oscillations is maximal,

$$j_{h,max} = \frac{\pi^2 k_{\mathrm{B}}^2 T_l^2}{6h} \frac{1 + \cos\phi}{3 + \cos\phi}$$
$$+ \frac{E_{Th}^2}{h} \frac{1 - \cos\phi}{3 + \cos\phi} \mathrm{Li}_2[\cos^2(\phi/2)], \tag{57}$$

where $\mathrm{Li}_2(z)$ is the polylogarithmic function $\mathrm{Li}_n(z) = \sum_{k=1}^{\infty} z^k/k^n$. The dependence of $j_h(\phi)$ on the flux is shown in Fig. 3 as a dashed curve. Depending on the Aharonov-Bohm phase the thermoelectric and heat currents can flow in the opposite $(0 < \phi < \pi)$ or in the same $(\pi < \phi < 2\pi)$ direction. One sees that the heat current j_h is maximal at $\phi = 0$ with the value,

$$j_h(0) = \frac{\pi^2 k_{\mathrm{B}}^2 T_l^2}{12h} (T_l^2 - T_r^2), \tag{58}$$

which is half of the ballistic heat current of complex 1D fermions. The heat current is zero at $\phi = (2n+1)\pi$. The origin of the zeros of j_h becomes transparent after one represents the Dirac ψ operators in the normal region using a Majorana basis γ_1, γ_2,

$$\gamma_1 = (\psi + \psi^+)/\sqrt{2}, \qquad \gamma_2 = -i(\psi^+ - \psi)/\sqrt{2}. \tag{59}$$

The total phase $\phi = \phi_{AB} + \sum_i^4 \alpha_i = \pi$ can be interpreted as the sum of a zero Aharonov-Bohm phase and a set of redefined α_i's, for instance, with $\alpha_l = \alpha_1 = \alpha_2 = \pi/2$ and $\alpha_r = \alpha_3 = \alpha_4 = 0$. The scattering among χ, γ_1, and γ_2 for such contacts with equal phases α of Y junctions was found in Ref. [18]
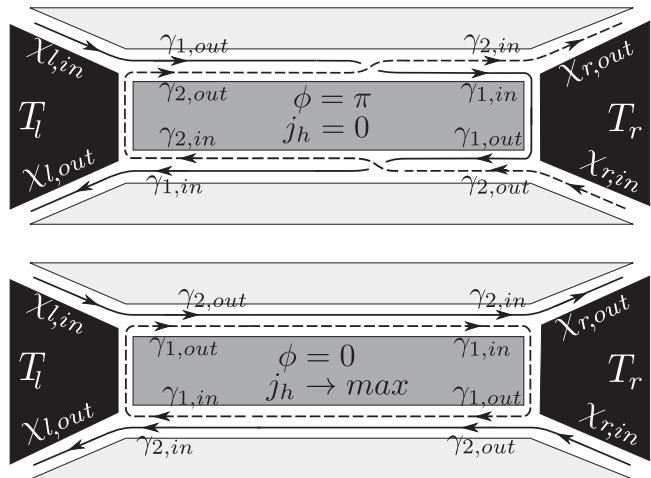

FIG. 5. Scattering in the basis of the neutral modes χ, γ_1, and γ_2 at a zero heat current (upper panel with $\phi = \pi$) and at the maximum heat current $j_h = \frac{\pi^2 k_{\mathrm{B}}^2}{12h}(T_l^2 - T_r^2)$ (lower panel with $\phi = 0$).

Eq. (37),

$$\begin{bmatrix} \gamma_{1,\mathrm{out}} \\ \chi_{\beta,\mathrm{out}} \\ \gamma_{2,\mathrm{out}} \end{bmatrix} = \begin{bmatrix} \cos^2\alpha_\beta & -\sin\alpha_\beta & -\frac{\sin 2\alpha_\beta}{2} \\ -\sin\alpha_\beta & 0 & -\cos\alpha_\beta \\ \frac{\sin 2\alpha_\beta}{2} & \cos\alpha & -\sin^2\alpha_\beta \end{bmatrix} \begin{bmatrix} \gamma_{1,\mathrm{in}} \\ \chi_{\beta,\mathrm{in}} \\ \gamma_{2,\mathrm{in}} \end{bmatrix}, \tag{60}$$

with the index $\beta = l,r$. From this representation of the scattering matrices for the left and right contacts, i.e., for $\alpha_l = \pi/2$ and $\alpha_r = 0$, we find the paths of the scattered neutral modes as shown in Fig. 5. The incoming $\chi_{l,\mathrm{in}}$ mode in the left lead converts into γ_1, propagates to the right lead, scatters in the normal region, and flows back to the left edge. There is no mixing between γ_1 (solid curve) and γ_2 (dashed curve) and no energy exchange between the two SCs. Hence, the heat current is zero. In the opposite case of the maximal heat current, which is equivalent to $\alpha = \alpha_l = \alpha_r = 0$, the mode $\chi_{l,\mathrm{in}}$ converts into γ_2 in the left lead and flows away as $\chi_{r,\mathrm{out}}$ in the right one.

VII. CONCLUSIONS

We have analyzed the thermoelectric and heat transport in a long 1D ballistic Josephson junction where the leads are formed by gapless chiral Majorana channels. Such a junction can be realized as a hybrid structure based on a 3D topological insulator surface in the proximity with s-wave superconducting and magnetic films. The interfaces of the gapped sectors support neutral and charged 1D chiral liquids. The normal region is formed by two chiral Dirac liquids spaced by a magnetic material. The chiral contact is formed by four Y junctions which serve as Dirac-Majorana converters. Our crucial assumption is that the Thouless energy, proportional to the inverse dwell time in the interferometer, is much lower than the superconducting and exchange gaps.

We have obtained the following results. (i) We have generalized the current-phase relation from our previous work [18] to nonidentical Dirac-Majorana contacts and discovered

a nonzero Josephson current in the absence of the phase bias, the Aharonov-Bohm phase, and the temperature gradient. (ii) We have calculated the thermoelectric current and (iii) the heat current as functions of the magnetic flux and the temperatures of the leads. An important difference of the chiral contact from junctions based on a 2D TI, quantum-Hall bar, or a spin-orbit coupled nanowire is the absence of a quasiparticle gap in the leads due to the gapless Majorana modes. This results in the absence of the temperature threshold in the current-flux relations. We observe a nonsinusoidal $2\Phi_0$-periodic dependence of the thermoelectric and heat currents on the magnetic flux. The maximum oscillation amplitude of the thermoelectric current is proportional to $eE_{Th}/\hbar$ and scales as one over the device size. The maximal amplitude is achieved at a low temperature in one of the superconductors and a high temperature in the other one, i.e., at $T_l \gg E_{Th} \gg T_r$ or $T_r \gg E_{Th} \gg T_l$. The heat current oscillates between zero and a value that corresponds to one-half of the heat conductance quantum.

[1] A. Y. Kitaev, Phys.-Usp. **44**, 131 (2001).

[2] C. Nayak, S. H. Simon, A. Stern, M. Freedman, and S. Das Sarma, Rev. Mod. Phys. **80**, 1083 (2008).

[3] For a review of proposed states, see G. Yang and D. E. Feldman, Phys. Rev. B **88**, 085317 (2013).

[4] P. T. Zucker and D. E. Feldman, Phys. Rev. Lett. **117**, 096802 (2016).

[5] D. E. Feldman and F. Li, Phys. Rev. B **78**, 161304(R) (2008).

[6] A. Seidel and K. Yang, Phys. Rev. B **80**, 241309(R) (2009).

[7] C. Wang and D. E. Feldman, Phys. Rev. B **81**, 035318 (2010).

[8] L. Fu and C. L. Kane, Phys. Rev. Lett. **100**, 096407 (2008).

[9] L. Fu and C. L. Kane, Phys. Rev. Lett. **102**, 216403 (2009).

[10] X.-L. Qi and S.-C. Zhang, Rev. Mod. Phys. **83**, 1057 (2011).

[11] J. Alicea, Rep. Prog. Phys. **75**, 076501 (2012).

[12] Q. L. He, L. Pan, A. L. Stern, E. Burks, X. Che, G. Yin, J. Wang, B. Lian, Q. Zhou, E. S. Choi, K. Murata, X. Kou, T. Nie, Q. Shao, Y. Fan, S.-C. Zhang, K. Liu, J. Xia, and K. L. Wang, arXiv:1606.05712.

[13] G. C. Ménard, S. Guissart, C. Brun, M. Trif, F. Debontridder, R. T. Leriche, D. Demaille, D. Roditchev, P. Simon, and T. Cren, arXiv:1607.06353.

[14] A. R. Akhmerov, J. Nilsson, and C. W. J. Beenakker, Phys. Rev. Lett. **102**, 216404 (2009).

[15] K. T. Law, P. A. Lee, and T. K. Ng, Phys. Rev. Lett. **103**, 237001 (2009).

[16] J. Li, G. Fleury, and M. Büttiker, Phys. Rev. B **85**, 125440 (2012).

[17] G. Strübi, W. Belzig, M. S. Choi, and C. Bruder, Phys. Rev. Lett. **107**, 136403 (2011).

[18] D. S. Shapiro, A. Shnirman, and A. D. Mirlin, Phys. Rev. B **93**, 155411 (2016).

[19] C.-Y. Hou, K. Shtengel, and G. Refael, Phys. Rev. B **88**, 075304 (2013).

[20] J. P. Ramos-Andrade, O. Ávalos-Ovando, P. A. Orellana, and S. E. Ulloa, Phys. Rev. B **94**, 155436 (2016).

[21] J. A. M. van Ostaay, A. R. Akhmerov, and C. W. J. Beenakker, Phys. Rev. B **83**, 195441 (2011).

[22] A. Y. Zyuzin, Phys. Rev. B **50**, 323 (1994).

[23] F. Amet, C. T. Ke, I. V. Borzenets, J. Wang, K. Watanabe, T. Taniguchi, R. S. Deacon, M. Yamamoto, Y. Bomze, S. Tarucha, and G. Finkelstein, Science **352**, 966 (2016).

[24] S.-P. Lee, K. Michaeli, J. Alicea, and A. Yacoby, Phys. Rev. Lett. **113**, 197001 (2014).

[25] G. Tkachov, P. Burset, B. Trauzettel, and E. M. Hankiewicz, Phys. Rev. B **92**, 045408 (2015).

[26] B. Baxevanis, V. P. Ostroukh, and C. W. J. Beenakker, Phys. Rev. B **91**, 041409(R) (2015).

[27] S. V. Mironov, A. S. Mel'nikov, and A. I. Buzdin, Phys. Rev. Lett. **114**, 227001 (2015).

[28] B. Sothmann and E. M. Hankiewicz, Phys. Rev. B **94**, 081407(R) (2016).

[29] B. Sothmann, F. Giazotto, and E. M. Hankiewicz, New J. Phys. **19**, 023056 (2017).

[30] N. V. Gnezdilov, B. van Heck, M. Diez, J. A. Hutasoit, and C. W. J. Beenakker, Phys. Rev. B **92**, 121406(R) (2015).

[31] S. Jezouin, F. D. Parmentier, A. Anthore, U. Gennser, A. Cavanna, Y. Jin, and F. Pierre, Science **342**, 601 (2013).

[32] M. Banerjee, M. Heiblum, A. Rosenblatt, Y. Oreg, D. E. Feldman, A. Stern, and V. Umansky, Nature (London) **545**, 75 (2017).

[33] L. Jiang, D. Pekker, J. Alicea, G. Refael, Y. Oreg, and F. von Oppen, Phys. Rev. Lett. **107**, 236401 (2011).

[34] L. Fu and C. L. Kane, Phys. Rev. B **79**, 161408(R) (2009).

[35] D. M. Badiane, M. Houzet, and J. S. Meyer, Phys. Rev. Lett. **107**, 177002 (2011).

[36] C. W. J. Beenakker, D. I. Pikulin, T. Hyart, H. Schomerus, and J. P. Dahlhaus, Phys. Rev. Lett. **110**, 017003 (2013).

[37] P. A. Ioselevich and M. V. Feigel'man, Phys. Rev. Lett. **106**, 077003 (2011).

[38] V. Mourik, K. Zuo, S. M. Frolov, S. R. Plissard, E. P. A. M. Bakkers, and L. P. Kouwenhoven, Science **336**, 1003 (2012).

[39] Y. M. Blanter and M. Büttiker, Phys. Rep. **336**, 1 (2000).

[40] A. Buzdin, Phys. Rev. Lett. **101**, 107005 (2008).

[41] E. Goldobin, D. Koelle, R. Kleiner, and R. G. Mints, Phys. Rev. Lett. **107**, 227001 (2011).

[42] H. Sickinger, A. Lipman, M. Weides, R. G. Mints, H. Kohlstedt, D. Koelle, R. Kleiner, and E. Goldobin, Phys. Rev. Lett. **109**, 107002 (2012).

[43] M. Alidoust and J. Linder, Phys. Rev. B **87**, 060503(R) (2013).

[44] A. Zyuzin, M. Alidoust, and D. Loss, Phys. Rev. B **93**, 214502 (2016); I. V. Bobkova, A. M. Bobkov, A. A. Zyuzin, and M. Alidoust, *ibid.* **94**, 134506 (2016).

[45] C. Winkelholz, R. Fazio, F. W. J. Hekking, and G. Schön, Phys. Rev. Lett. **77**, 3200 (1996).

[46] D. L. Maslov, M. Stone, P. M. Goldbart, and D. Loss, Phys. Rev. B **53**, 1548 (1996).

[47] R. Fazio, F. W. J. Hekking, and A. A. Odintsov, Phys. Rev. B **53**, 6653 (1996).

[48] P. Dubos, H. Courtois, B. Pannetier, F. K. Wilhelm, A. D. Zaikin, and G. Schön, Phys. Rev. B **63**, 064502 (2001).

[49] A. Levchenko, A. Kamenev, and L. Glazman, Phys. Rev. B **74**, 212509 (2006).